

## Aircraft experiments with visible and infrared sensors

A. WADSWORTH

Groupeement pour le Développement de la Télédétection Aérospatiale (GDTA),  
18 Avenue Edouard-Belin, 31055 Toulouse Cedex France, Institut Français du  
Pétrole, BP 311, 92506 Rueil Malmaison Cedex, France

W. J. LOOYEN

National Lucht-en-Ruimtevaartlaboratorium (NLR), Space Division, Remote  
Sensing Department, P.O. Box 153, 8300 AD Emmeloord, The Netherlands

R. REUTER

Physics Department, Universität Oldenburg, Postfach 2503, D-2900 Oldenburg,  
Germany

M. PETIT

Institut Français de Recherche Scientifique pour le Développement en  
Coopération, BP 5045, 34032 Montpellier Cedex, France

**Abstract.** Visible and near-visible sensors, which have been widely used in the beginning of the period of interest, have been later overshadowed by the availability of sensors using the microwave part of the spectrum. However, the latter years of this period have shown an obvious come-back with numerous experiments flown with new generation equipment. This paper describes briefly the first generation sensors and how they were used in airborne experiments, explains the developments being conducted from mechanical to push-broom scanners and to non-scanning sensors, shows how some sensors were being integrated in comprehensive systems and what is the trend found in the later years of the period of reference. This is illustrated by examples of existing equipment in France and in Europe, and two case studies: one on the Dutch CAESAR push-broom scanner, the other on the Oceanographic Lidar System developed by the University of Oldenburg in Germany.

### 1. Introduction

It is rather difficult to be exhaustive in dealing with aircraft experiments with visible and infrared sensors. However, we shall describe sensors and experiments that have been of major interest either because they have led to the development of major equipment, or because they have been a noteworthy, or a particular step, in the development of airborne remote sensing.

In addition to these general aspects of airborne remote sensing we shall look, in more detail, at two airborne sensors that correspond to the direction of research; a passive imaging one, the Dutch Charge-Coupled Device (CCD) push-broom Airborne Experimental Scanner for Applications in Remote sensing (CAESAR), and an active one, the German Oceanographic Lidar System (OLS), because they represent major techniques that have become operational.

### 2. Developments since the seventies

Airborne remote sensing at the beginning of the 1970s was mainly using airborne aerial photography, along with thermal or visible scanning systems.

0143-1161/92 \$3.00 © 1992 Taylor & Francis Ltd

O.R.S.T.O.M. Fonds Documentaire

N° B 35710

14 DEC. 1992

Cote PW ex L M

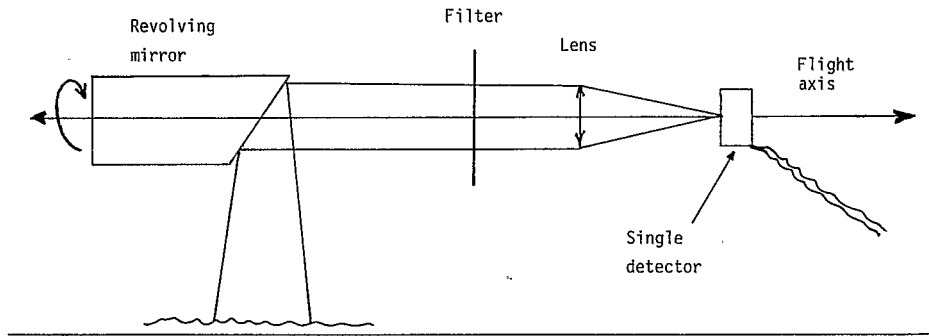


Figure 1. Sketch of a mechanical scanner.

### 2.1. Sensors: from mechanical to push-broom scanning

The imaging sensors at the beginning of the remote sensing era were of one single type: the mechanical scanner. As can be seen in figure 1, the instrument which has its longitudinal axis along the flight line looks at the nadir, the lateral scanning being achieved via a revolving mirror set at 45°. At the end of the sensor, a detector, a single one for a single channel sensor, or a multiple set after a filter, and a prism or a grating for a multichannel sensor, gives a signal related to the landscape 'overflowed' (Colwell 1983). Successive scan lines are obtained because, between one scan and the next, the aircraft has flown the corresponding distance between two successive image lines.

This signal after detection was then either recorded on photographic paper or on analogue tape. There was, at that time, no digital recording and digitizing during play-back was very unusual. The interpreter was working with a paper print with a low radiometric accuracy or resolution. Later the signal was digitized upon play-back or in some cases directly recorded in a digital form.

Video cameras were also developed as airborne sensors when they became lighter, cheaper and more rugged. They were used in association with a video recorder, as general sensor, to see quickly where the flight lines were located. In some cases, however, a special use of them was made as Low Light Level TV cameras (LLTV), sometimes in oil slick surveillance and often for the detection and identification of the trespasser.

Thanks to developments in microelectronics, a new type of sensor began to be developed and used in airborne experiments, the push-broom, using CCD detectors. This sensor has no moving parts and records the whole image line at one time.

The CCD is an integrated circuit of Metal Oxide Semi-conductors (MOS) technology containing potential wells or cells that can accumulate electrical charges. The electrical charges are created by individual photodiodes that are exposed to the incoming radiation (figure 2). After the exposure period, the accumulated photoelectrons are transferred to a readout stage. Transfer is achieved by modifying the potential barrier between the wells, allowing the charge packets to shift sequentially towards an output circuit, to be converted into voltages. In a linear CCD image sensor, such as the one that is applied in CAESAR, or other airborne and spaceborne sensors, the charge from the detectors is initially transferred to the parallel inputs of two shift registers connected to alternate detectors. When a line of

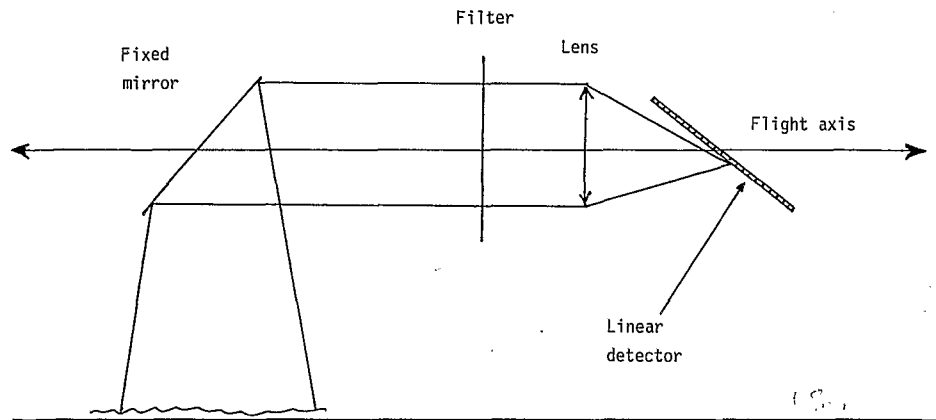


Figure 2. Sketch of a linear push-broom scanner.

data is completely transferred to the shift registers the detectors are reset and ready to accumulate a new line of data.

Apart from a bias, the number of generated photoelectrons is proportional to the integrated amount of radiation, the ratio being dependent on the sensitivity of the individual detectors. The noise bias is usually expressed as the dark current of the detector, which is the electrical charge accumulated during a period when the photodiode is not exposed to the radiation. Both the sensitivity and the dark current of the detectors have to be known in order to relate the measured signal to the incident radiation.

The application of linear detector arrays to multispectral imaging has the following advantages in comparison with classical mechanical scanning techniques.

1. Substantial increase of the integration time by which the spatial resolution can be increased.
2. Improved image quality in terms of geometry.
3. Absence of mechanical moving parts.

The disadvantages of this type of sensor are related to increased requirements for image quality in the focal plane of the main optics and the radiometric calibration required for all individual detector elements (1728 or more per integrated circuit). Moreover, for most commercially available CCD detectors, the wavelength range is limited to the range between 400 and 1100 nm. If more than one wavelength is needed then more than one linear array is needed and there is quickly a problem of sensor overcrowding in the focal plane of the sensor.

To overcome this latter problem, two-dimensional integrated circuits have been developed and used during recent experiments scanning an image line transversally and a frequency longitudinally. Figure 3 shows how such a device makes it possible to record data in numerous successive wavelengths at a time.

## 2.2. Operational equipment

Here again we do not plan to be exhaustive, but to show examples of what has been used in airborne experiments.

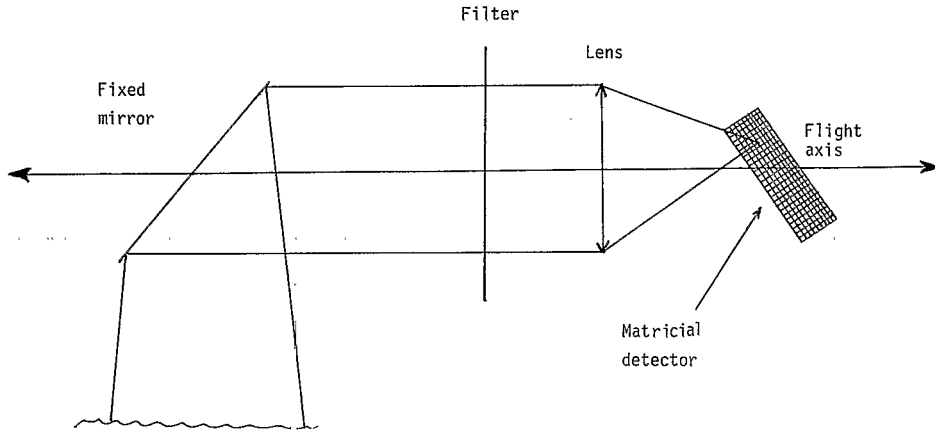


Figure 3. Sketch of a two-dimensional push-broom scanner.

### 2.2.1. Scanners

They are passive imaging sensors. In order to assess and compare the characteristics of different sensors, table 1 lists data of early mechanical scanners: the American Daedalus, working in the ultraviolet (UV), the visible and the near-infrared (IR) with 10 channels; the French Cyclope in the low thermal infrared and the French Laboratoire de Météorology Dynamique (LMD) Aries working in the high thermal infrared. All these sensors have been used in national or international experiments over land and sea, as explained later. Other information can be found, for example, in Massin (1978). As an example of more recent mechanical sensors, data on the Daedalus AADS 1268 are also given.

### 2.2.2. Video cameras

These sensors are passive imaging ones. They have been widely used, for example in an experiment called Topomex which was conducted during the Shuttle Imaging Radar (SIR-A) flights over the North Sea at the end of 1981, jointly by the Danish Companies Intradan, Terma, the Technical University of Denmark and Jørgen

Table 1. Examples of mechanical scanners.

Name	Analogue digital	Number of channels	Spectral bands ( $\mu\text{m}$ )	Field of view	IFOV† (mrad)	Scanning rate (cycles)
Daedalus DS-1230	A	10	0.38-1.10	77°20	2.5	80
Satellite Cyclope	A	1	3-6	114°	5	72
LMD Aries	D	1	10.5-12.5	90°	10	60
Daedalus AADS 1268	D	11	0.42-13.0		2.5 or 1.25	

† Instantaneous Field of View (IFOV).

Andersen Ingeniørfirma (JAI). The flights were achieved over oil slicks, using microwave sensors and two LLLTVs one in the visible and one in the UV. They were confirmed to be very good complements of the passive microwave sensor in the assessment of the total extent of the slicks and in the evaluation of their thicknesses. Their known susceptibility to light saturation was also confirmed. However, those quite simple sensors are now widely used by all the agencies involved in oil spill monitoring.

### 2.2.3. *Non-imaging sensors*

These can either be active or passive. An example of a passive one is given in the next section where a custom-made sensor based on a Barnes Precision Radiation Thermometer (PRT)-5 has been used for fishery surveys in the Atlantic, the Pacific and the Indian Oceans, with a wave band of 8-14  $\mu\text{m}$  or 9.5-11.5  $\mu\text{m}$ .

An example of an active device is also given later with the description and evaluation of the German Oceanic Radar System (OLS). The active part is a laser working either in the UV or the visible part of the spectrum.

## 2.3. *Experiments conducted*

### 2.3.1. *Early oil pollution detection and investigation*

Remote sensing experiments in Europe began with two main applications, (i) thermal infrared surveys of geological features and (ii) oil pollution detection and monitoring. We shall see here how this IR technique was tested at sea in the framework of multi-national experiments.

Between 1972 and 1976, Pollution en Mer (POLUMER) experiments were conducted jointly by French agencies: Institut Français du Pétrole (IFP), Centre National d'Exploitation des Océans (CNEXO), now Institut Français pour la Recherche et l'Exploration en Mer (IFREMER), the French navy, French and foreign oil companies, the Dutch National Lucht-en-Ruimtevaartlaboratorium (NLR), and others, with the aim in 1974, as far as remote sensing was concerned, to 'Select the most relevant sensors and techniques' that could be used in the French waters, in this case off Brittany, for the application to oil pollution monitoring. Different crude or gas oils were spilled, then mechanically and chemically treated by different techniques and monitored before, during and after treatment.

Those POLUMER experiments, and later the Protection Maritime (PROTECMAR) follow-on, were very interesting in assessing the potential and limits of the thermal infrared for this particular application, since they showed the time response of treated oil in the IR, in particular the vanishing of the signal during and soon after treatment and its later reappearance.

Thanks to these experiments and similar ones that were conducted mainly in Europe and North America, the IR imaging technique soon proved operational and specific airborne systems are now fully operational, comprising a side-looking radar for general surveillance, a thermal IR scanner for thickness evaluation, film and video cameras for tracking the trespasser and proof recording. This kind of system is available now for routine surveys in most of the European countries: for some years in Belgium, Holland, Germany, Italy and even in France where the French Customs operate a system installed by the Laboratoire National d'Essais (LNE) on board a Reims Aviation/Cessna F 406 aircraft equipped with a side-looking radar, a thermal IR scanner and a video camera, as shown in figure 4.



Figure 4. The French pollution surveillance system.

### 2.3.2. Airborne radiometry for tuna fish survey

The Institut Français de Recherche Scientifique pour le Développement en Coopération (ORSTOM) has conducted, between 1972 and 1983, experiments and surveys for the monitoring of tuna schools (Marsac *et al.* 1987).

Those flight operations represent a grand total of more than 4300 flight hours and have in common the study of the relation between a hydrologic environment and tuna concentrations. For each surveyed zone the thermal surface environment and the fishing context are different and surveys have been conducted over high contrast thermal zones in the Atlantic and New Zealand, medium ones in New Caledonia, Vanuatu and the western Atlantic and low ones in Polynesia and the Seychelles. Tuna fishing was also very active in the eastern Atlantic and in New Zealand, embryonic or non-existent in New Caledonia, French Polynesia or the Seychelles in 1982, or quickly expanding in the Seychelles after 1983.

A heavily modified and adapted Barnes PRT-5 non-imaging sensor looks at the sea surface via a hatch in the floor of the aircraft. The wavebands used, depending on the zone to be surveyed, were of 8–14  $\mu\text{m}$  or 9.5–11.5  $\mu\text{m}$ . First, the measured surface temperature was being recorded on paper, but later the signal was recorded via a Hewlett-Packard (HP) 85 microcomputer.

Initially, the operator had indicators of time, altitude, heading and speed, but later the aircraft's Omega Very Low Frequency (VLF) navigation system was linked to the digital recorder. Moreover, during the flight, every five minutes or when a special event occurred (a tuna school, a floating object, a thermal front, changes in the colour of the water, birds, marine mammals, boats fishing), the operator recorded the nature of the event, the time, the meteorological conditions, and the sea surface temperature after instrumental and atmospheric corrections. The position of the fishing flotilla was constantly monitored via radio links. On the latest version of the instantaneous position, heading, sea state, water colour, wind speed and direction

and distance of the observed schools from the track, are also recorded. The precision of the measured surface temperature has been found to be better than 0.2°C, which is considered sufficient for the application.

During the flight the boats can be directed towards interesting schools and the size of the catch can be estimated by the system operator in advance. After the flight a quick exploitation of the data set is conducted and this analysis leads to an estimation of the tuna surface stock. The limits of the method come from the fact that tuna fish are highly migratory species and move vertically in the water column. Other species have been investigated with this method and more research work is to be conducted with the help of thermal IR and microwave sensors.

### 2.3.3. SPOT simulation experiments

Before the successful launch of the Satellite Probatoire pour l'Observation de la Terre (SPOT) at the beginning of March 1986, numerous experiments were being conducted in order to be ready to use its data with maximum efficiency. A simulation programme was realized between 1980 and 1984 because past experiences had shown that considerable time was usually required to assess fully the properties and potential applications of a new sensor.

The Centre National d'Etudes Spatiales (CNES) developed two simulation approaches: (i) the geometrical approach and (ii) the radiometric approach. The first one involved simulation of the parameters that would affect the geometrical quality of the images, the later was achieved via flights conducted by GDTA in various parts of the world: Europe, Africa, Asia.

To achieve this, investigations on spectral bands, line of sight, local time influence and satellite track orientation were conducted using a Daedalus scanner with special filters and later a multispectral push-broom scanner built especially for that purpose. This instrument is a four channel optical sensor equipped with a tele centred head (each channel having a motorized lens aperture) neutral densities and spectral filter at the rear of the lens, a Thomson CCD linear detector and its associated electronics, and the mechanical setting for focus and line-up. The instrument is installed on a standard air photography optical mount.

Because of its purpose, three out of the four channels were set to the SPOT wavelengths, the green band of 510 to 600 nm, the red band of 610 to 720 nm and the near-IR band of 760 to 950 nm. The fourth waveband was set at a 450 to 510 nm window, in the blue, for oceanographic purposes. It was also possible to use narrow filters of 10 nm or to have broader wavebands. The digital signal was recorded on High Density Digital Tape (HDDT) with a 3.8 M.bits/s maximum data rate.

The flights conducted allowed a better knowledge of the performance of the then future satellite and the instrument is to be considered as a good example of a sensor built on purpose for experimental thematic and instrumental tests.

## 2.4. Trends

At the beginning of the period of reference the mechanical scanner was the most widely used sensor. During approximately the last ten years it suffered some kind of shadow from the development of microwave techniques, passive or active, which gave way to the operational use of the Side Looking Airborne Radar (SLAR) either in the real aperture mode, or in the Synthetic Aperture mode (SAR), or to the Passive Microwave Imager. However, it was found recently that the visible part of the spectrum was of great use, and that was proved by some spaceborne sensors like

the French SPOT, or the American Thematic Mapper (TM), and the new emerging microelectrooptics techniques have allowed an interesting come-back in the operational systems of the airborne sensors working in the visible and infrared parts of the spectrum.

### 3. Case study of a push-broom type scanner: CAESAR

#### 3.1. Introduction

In 1981 a project was proposed by the National Research Laboratory (NLR) and the Institute of Applied Physics of the Technical Research Centre of the Technical University of Delft (TNO-TUD) in The Netherlands, with the aim of developing an airborne multispectral push-broom scanner using linear CCD detector arrays. The project was funded by the Ministry of Education and Sciences, the Netherlands Remote Sensing Board (BCRS) and the participating institutes and was executed within the framework of the National Remote Sensing Programme. The multispectral scanner CAESAR and accompanying processing algorithms were completed in 1988.

The objectives of the project were to increase both technical knowledge of push-broom scanners and provide practical experience with the application of linear CCD detectors in remote sensing for land and sea observation. In addition an advanced airborne system would become available for research activities in the framework of the national programme.

#### 3.2. System lay-out

For trade-off studies, it was concluded that the optimum configuration would be a cluster of four single-lens-triple-CCD-channel cameras. The four cameras are integrated in one fixture. Two modules can be distinguished. First the down-looking module, consisting of three cameras placed in a line. Secondly the forward-looking module, consisting of the fourth camera. Each basic camera consists of a lens, a three CCD array focal plane assembly, a filter tray and some electronics. The focal plane assembly uses two small prisms to deflect the light to the two outer CCD arrays [figures 5 (a) and (b), (Pouwels 1987)].

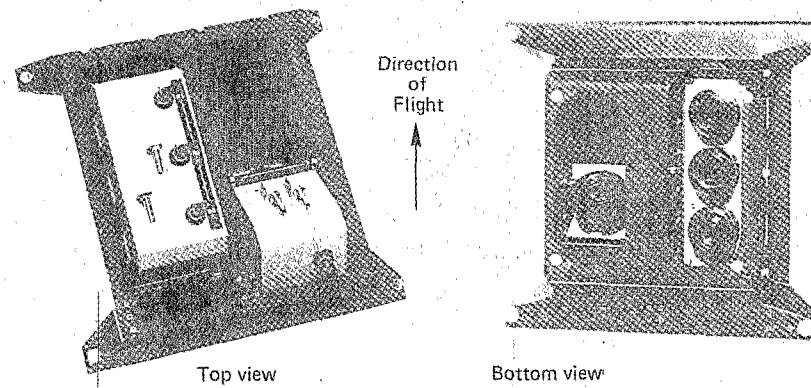


Figure 5(a). Top view and bottom view of the CAESAR scanner with the down-looking and forward-looking module integrated in one fixture.

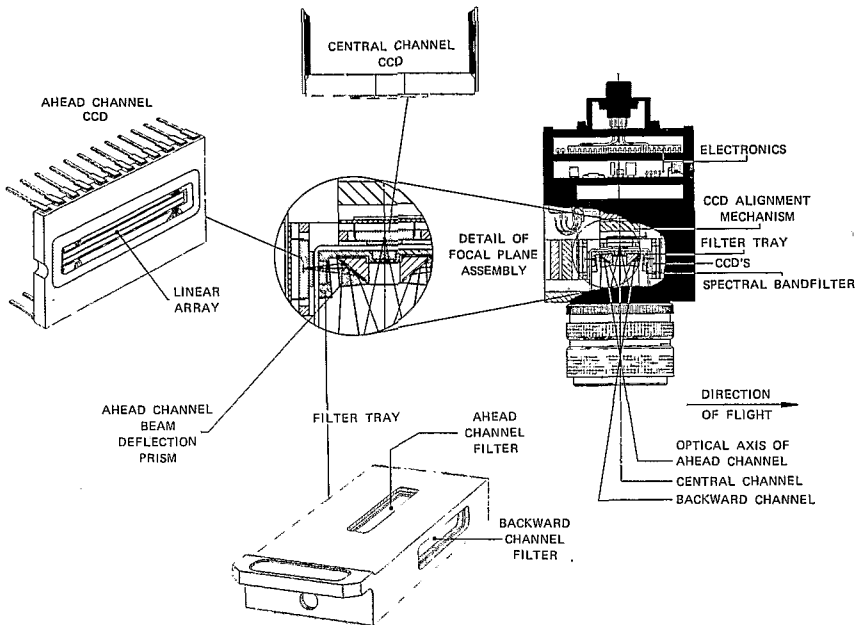


Figure 5(b). CAESAR basic triple CCD camera.

Each CCD array [Thomson Compagnie Générale de Telegraphie sans Fils (CSF) TH7801] consists of 1728 photosensitive elements of  $13$  by  $13\ \mu\text{m}$  and about 20 reference elements. The sensitive elements have individual sensitivity values and dark current values. The reference elements are used to determine the in-flight electrical zero reference for the signals and the in-flight dark current values. The analogue signals from the CCDs are digitized with a 12-bit resolution matched to the dynamics of the CCD, independent of the actual, measured signal. Digital values are recorded on a special high density tape.

User requirements mainly concerned the selection of the position, width and number of spectral bands, dynamic range, radiometric resolution and spatial resolution. On the basis of these requirements four operation modes were identified.

1. Land mode (land observation).
2. Special land mode (land observation, high spatial resolution).
3. Forward-looking mode (land observation).
4. Sea mode (sea/water) observation).

The spectral response of the arrays is governed by narrow bandpass filters constructed of interference filters in combination with absorption filters. Two standard filter sets (for land and sea, respectively) are currently available and other filter sets can be defined. The land filter set (table 2) is a double set. One filter set serves the three central arrays in the land mode and special land mode. The second set serves the three arrays of the forward-looking module.

The sea filter set (table 3) is used with all nine arrays of the down-looking module. The wavelengths and bandwidths are identical to the ones proposed for the Ocean Colour Monitor (OCM), which was a potential optical instrument for a

Table 2. The Caesar Push-Broom Scanner. Characteristic central wavelengths and bandwidths for the land mode, special land mode and forward-looking mode.

Array code	Wavelength (nm)	Bandwidth (nm)
D1C/F1B	550	30
D2C/F1A	670	30
D3C/F1C	870	50

The array code identifies the channel in the CAESAR coding system. In the first position, D stands for Down and F stands for Forward. The figures in the middle indicate the camera in the module and A/C/B stands for Ahead/Central/Backwards which indicate the arrays in the camera.

future remote sensing satellite of the European Space Agency (ESA). One channel is duplicated in spectral response but has a different view angle.

CAESAR is mounted fixed above the optical window in the fuselage of NLR's Metro II research aircraft. The optical axis of the down-looking module is pointing towards the earth and perpendicular to the longitudinal and lateral axis of the aircraft. The optical axis of the forward-looking module forms an angle of  $52^\circ$  with the optical axis of the down-looking module. All CCD channels are parallel to the lateral axis of the aircraft.

The instantaneous fields of view are 0.25 mrad and 0.15 mrad for the down-looking module and for the forward-looking module, respectively. The channel orientation is the same in both the land mode and the special land mode. The three central arrays (channels) of the down-looking module are used. Owing to the geometric calibration of the cameras, co-registration of the three channels does not require any further processing in the preprocessing stage.

The forward-looking module has a nominal offset angle of  $52^\circ$  with respect to the untilted down-looking module. The three different channels forming the forward-looking module are pointing forward with angles of  $45^\circ$ ,  $52^\circ$  and  $59^\circ$ , respectively. The focal length of the lens is adapted to the greater object distance.

In the special land mode a shorter integration time is used, which results in an increased spatial resolution of 0.5 by 0.5 m at a flight altitude of 2000 m.

In the sea mode all nine arrays of the three cameras of the down-looking module are in use. The ahead arrays are pointing  $11.5^\circ$  forward, the central arrays are

Table 3. The Caesar Push-Broom Scanner. Characteristic central wavelengths and bandwidths for the sea mode

Array code	Wavelength (nm)	Bandwidth (nm)
D1B	410	20
D1A	445	20
D1C	520	20
D2B	565	20
D2A	630	20
D2C	685	20
D3C	785	30
D3A/D3B	1020	60

pointing towards the Earth and the backward arrays are pointing  $11.5^\circ$  backward. Because the cameras were calibrated for geometry, co-registration of the three ahead-channels does not require any further processing in the preprocessing stage. The three central channels and backward channels are also co-registered this way. The co-registration of an ahead channel and a backward channel is performed at the NLR Remote Sensing Data processing system (RESEDA).

Another feature of CAESAR is the possibility of tilting the down-looking module over an angle varying from  $0^\circ$  to  $20^\circ$  in order to avoid sunglint. This feature is relevant for the sea mode operation of CAESAR. All configurations are presented in table 4.

### 3.3. Data preprocessing

In 1980 the BCRS had taken the initiative to form the working group Pre-processing Airborne Remote Sensing (PARES) to derive system corrections for airborne microwave remote sensing imagery. Such corrections are necessary to compensate for aircraft motion and attitude as well as for specific sensor distortions. The working group developed a preprocessing software package PARES. For the pre-processing of CAESAR data, NLR developed a special version of PARES for Optical Remote Sensing data, called OPTIPARES (Optical Processing of Airborne Remote Sensing). In the case of CAESAR specific sensor corrections deal with the optical aspects of the scanner and the radiometric calibration required for all individual elements and for all CCD-arrays. The OPTIPARES programme performs a radiometric and a geometric correction.

### 3.4. Radiometric performance

Relative radiometric calibration is required for the quantitative comparison of data corresponding with a single multispectral image and with the temporal series of multispectral images. In the case of absolute radiometric calibration, the transfer

Table 4. The Caesar Push-Broom Scanner. Configurations for the land and sea modes.

	Land mode	Special land mode
Altitude (km)	3	2
Integration time (ms)	7.5	5
Ground speed (m/s)	100	100
Number of pixels	1728	1280
Swath width (m)	1296	640
Spatial resolution (m)	$0.75 \times 0.75$	$0.5 \times 0.5$
Quantization (bits)	10	9
	Sea mode	Forward-looking mode
Altitude (km)	6	3
Integration time (ms)	40	7.5
Ground speed (m/s)	105	100
Number of pixels	1728	1728
Swath width (m)	2592	$\pm 1400$
Spatial resolution (m)	$4.0 \times 4.0$	$2.0 \times 2.0$
Quantization (bits)	12	10

function is known between the spectral radiance at the entrance pupil of the instrument and the measured detector signal. Within the accuracy limits that can be achieved, an absolutely calibrated scanner can be used for multispectral radiance measurements. Absolute calibration is only required if the user wants to apply radiometric corrections by means of external data (from other instruments or models) and for the retrieval of object parameters from physically defined radiance values.

The CAESAR system was calibrated both relatively and absolutely and is able to detect a ground reflectance variation noise equivalent  $Ned\rho < 0.5$  per cent and  $Ned\rho < 0.05$  per cent over land and over sea respectively, but calibration of all the individual elements of the linear CCD array is required. Each of the 1728 elements of the different arrays is characterized by a specific sensitivity to the input radiance and a specific dark current.

The normalization factor and the dark current of the individual elements are determined in a factory set-up (van Valkenburg 1985). The calibration procedure results in a look-up table for each spectral band, containing the normalization factors and the dark current corrections for the individual CCD elements. This look-up table is used by the OPTIPARES programme during the pre-processing of the scanner data. The performance of CAESAR in terms of radiometric resolution was investigated using multispectral images that were recorded by CAESAR. For these scenes it can be assumed that averaging the input radiance (for each separate wavelength band) along the columns (constant element number) will yield a mean line of the image, along which only a low-frequency variation of the radiance can be expected. Since the high frequency features of the scene will be lost by the averaging process, the residual variation of the mean radiance going from element to element may be regarded as a measure of the calibration accuracy. Instrumental effects are neglected as it is assumed that they are also blurred out by the averaging because of their stochastic nature.

Using the mean radiance value  $L$  of the image the minimum detectable radiance difference,  $NedL$ , can be determined. In order to convert the value of  $NedL$  to a minimum detectable ground reflectance variation  $Ned\rho$ , the relation between the reflectance variation and the observed radiance variation has to be used. In general this relation will be a function of the wavelength and the observation conditions. This relation is modelled and calculations are made for different wavelengths and observation conditions. From these calculations the ratios between the reflectance variation and the observed radiance variation

$$dL_{\text{obs}}/(Ned\rho)_0$$

for the spectral bands of CAESAR were derived. These ratios were calculated for unfavourable observation conditions: Sun zenithal angle of  $65^\circ$ , visibility 5 km, edge of the field of view.

Table 5 summarizes the results of the evaluation of the performance of CAESAR in the sea mode. As can be seen from the table the radiometric resolution expressed by the  $Ned\rho$ , meets the requirement of 0.05 per cent for all channels except for the 410 nm channel. This result is in agreement with earlier predictions on the performance of CAESAR. Calibration of the 410 nm channel appeared to be very difficult because of the combined effect of low sensitivity of the CCDs in this wavelength band and a low input signal. Therefore normalization constants for this channel could not be determined with sufficient accuracy. Table 5 also summarizes the results

Table 5. Radiometric performance of the CAESAR Push-Broom Scanner expressed in noise equivalent delta-rho ( $Ned\rho$ ) for different operation modes.

Array code	$\lambda$ nm	$\sigma_{raw}$ %	$\sigma_{cor}$ %	$L_{obs}$	$L_{FS}$	$NedL$	$\frac{dL}{(Ned\rho)_0}$	$Ned\rho$ %
				W/m <sup>2</sup> /sr/ $\mu$ m				
<i>Sea mode</i>								
D1A	445	0.91	0.33	25.98	78	0.061	140	0.04
D1C	520	1.20	0.17	29.64	31	0.036	160	0.02
D1B	410	0.82	0.84	22.69	204	0.135	104	0.13
D2A	630	0.86	0.27	23.27	41	0.044	154	0.03
D2C	685	0.90	0.44	20.42	38	0.064	144	0.05
D2B	565	0.89	0.13	32.43	40	0.030	162	0.02
D3A	1020	1.46	1.04	4.06	200	0.030	78	0.04
D3C	785	0.80	0.33	9.76	26	0.023	122	0.02
D3B	1020	0.95	0.68	5.56	189	0.028	78	0.04
<i>Land mode</i>								
D1C	550	1.10	0.28	28.63	128	0.057	188	0.14
D2C	670	0.86	0.46	18.85	137	0.061	164	0.27
D3C	870	0.85	0.51	10.61	168	0.038	114	0.50
<i>Special land mode</i>								
D1C	550	1.43	0.86	15.05	192	0.090	188	0.31
D2C	670	1.37	1.00	11.15	205	0.080	164	0.45
D3C	870	0.95	0.57	45.34	252	0.180	114	0.45
<i>Forward-looking mode</i>								
F1A	670	1.02	0.66	30.26	346	0.140	164	0.49
F1C	870	0.88	0.39	40.88	170	0.110	114	0.20
F1B	550	0.90	0.39	33.60	248	0.090	188	0.18

$L_{obs}$  is the observed radiance for the test images,  $L_{FS}$  is the full-scale radiance and  $NedL$  is the pixel-to-pixel variation in the average observed radiances.  $NedL$  is the minimum detectable radiance difference,  $dL/(Ned\rho)_0$  is the ratio between the reflectance variation and the radiance variation.

of a similar analysis on the performance of CAESAR in the other three modes (land, special land and forward-looking). As can be seen from the table, these CAESAR modes also meet the requirements ( $Ned\rho < 0.5$  per cent). It should be noted that the number quoted for  $Ned\rho$  is valid for a radiance of 50 per cent of the full scale, where the error on the radiance measurement due to quantization can be neglected with respect to the normalization error. The values quoted were obtained simply by scaling the  $Ned\rho$  values that were found for the real observed radiance.

### 3.5. Geometric performance

In cooperation with the Faculty of Geodesy of the Delft University of Technology the geometric accuracy of CAESAR imagery was investigated. A comparison was carried out by two geodetic methods.

1. Affine transformation.
2. Two-dimensional similarity transformation.

Image coordinates in the CAESAR images were measured at the NLR by RESEDA using a digitizing unit. After displaying the image on the screen, points on the screen

Table 6. The CAESAR Push-Broom Scanner. Standard deviations of image coordinates with respect to RD coordinates after affine transformation and similarity transformation.

Standard deviation	Affine transformation (m)	2-D similarity transformation (m)
X-direction	1.2	2.5
Y-direction	3.3	4.2

(image coordinates) and corresponding points from a topographic map [Dutch Reference (DR) coordinates] were selected. From the two coordinate lists the parameters of both methods were calculated and the DR coordinates of the image points were estimated. A comparison of the differences between the estimated DR coordinates and the true DR coordinates gave standard deviations as listed in table 6.

Plots of the residual errors for both methods show that no structure is present in the residual errors. Examples of imagery are shown in figures 6 and 7.

### 3.6. Concluding remarks

The Netherlands can now offer the remote sensing community an advanced airborne push-broom scanner for land and marine applications. Both geometric and radiometric performance tests show that major user requirements are met.

In 1988 several projects were defined with the aims of evaluating the potential of the CAESAR scanner and of demonstrating its capabilities for remote sensing research. The studies, of which the results are published (Looyen *et al.* 1989), were carried out by a variety of remote sensing scientists. First results show that, in contrast to digitized aerial photography, calibrated CAESAR (land mode) data allow quantitative analysis of vegetation types. From the CAESAR sea-mode observations it follows that radiance measurements are in qualitative agreement with *in situ* measured yellow substance and chlorophyll concentrations. In 1989-90 several projects were executed with respect to vegetation stress mapping, water quality monitoring and the topographic potential of the CAESAR scanner.

## 4. The oceanographic lidar system

The airborne hydrographic lidar is an active sensor consisting of a laser emitting short pulses at near-UV or visible wavelengths, which are deflected towards the water surface and of a gated signal receiver for the detection of laser-induced radiation (table 7). Compared to passive radiometry, two main differences are

Figure 6. CAESAR special land mode image of the Dutch nature reserve 'de Weerribben'. The geometric correction process can be illustrated by the blackish stripes due to malfunctioning of some CCD elements. These stripes indicate the aircraft motion. However, the geometry of the terrain, due to the geometric correction process, is represented correctly. The software now excludes the malfunctioning elements from the geometric correction process. The scale of the original image is 1:5000.

Figure 7. CAESAR special land mode image of a coastal strip near the city of Oostvoorne, representing three spectral bands in a false colour image. The spatial resolution is 0.5 by 0.5 m. The scale of the original image is 1:10 000.



Table 7. The Oceanographic Lidar System (OLS).

<i>Excitation</i>		
Lasers	Excimer	Dye
Wavelength (nm)	308	450/533
Pulse length (ns)	12	6
Peak power (MW)	10	1
Rep. rate (Hz)		≤ 10
Footprint at 800 ft flight height (m)	2.5	0.7
<i>Detection</i>		
Telescope (m)	<i>f</i> /10 Schmidt-Cassegrain, diameter 0.4 m	
Wavelength selection	Dichroic splitters, interference filters and blocking filters	
Wavelengths (nm)	344 Water Raman @ <sub>ex</sub> = 308 and Gelbstoffe background	
	366 Gelbstoffe fluorescence	
	380 Gelbstoffe fluorescence	
	500 Gelbstoffe fluorescence	
	533 Water Raman @ <sub>ex</sub> = 450	
	650 Gelbstoffe fluorescence	
	685 Chlorophyll-a fluorescence	
Detectors	Photomultipliers EMI 9812/9818, gated	
Digitizer	Biomation 6500, 500 MHz, 6-bit [On the depth resolving lidar mode a fast logarithmic amplifier with 10 ns/decade fall time to enhance the dynamic range]	
System computer	LSI 11/23 with floppy disk, hard disk and magnetic tape	
Total weight	500 kg	

obvious. (i) The method is not dependent on sunlight: operation at night time yields even better signal-to-noise level since daylight background does not interfere with the laser-induced signals. (ii) Owing to the use of monochromatic laser light, and the registration of scattering fluorescence, it is possible to gather specific information on optical parameters or fluorescent substances in the upper water layers.

In this section some results obtained with the OLS of the University of Oldenburg are reviewed. This instrument was developed in 1983–84 with support of the Federal Minister for Research and Technology, Bonn, and operated in Dornier (Do) 28 and Do 228 research aircraft of the Deutsche Forschungs- und Versuchsanstalt für Luft- und Raumfahrt (DLR), Oberpfaffenhofen, previously DFVLR.

The instrument has been specifically designed for oceanographic research. Maps of water column parameters in coastal zones can be obtained synoptically since measuring times are short as compared with the characteristic time scales of hydrographic changes as, for example, the tidal period. A second area of application that has been studied in detail is the fluorometric analysis of oil spills in turbid coastal waters where strong fluorescence contributions from natural seawater compounds are also present.

A main characteristic of the lidar as an optical radar is its capability of deriving range-resolved data from time-resolved measurements of the signal return. Range resolution is a function of the laser pulse width and the bandwidth of the detection

system. In the development of the OLS special attention has been paid to the time-resolving capability, with the aim of evaluating depth profiles of water column parameters. With this instrument depth profiles of turbidity were obtained for the first time in 1984 in the northern Adriatic down to a water depth of 17 m, which corresponds to six attenuation lengths (Diebel-Langohr *et al.* 1986). In the following years profiles of turbidity and Gelbstoffe were derived in the German Bight (Diebel 1987) with 70 cm resolution.

However, the depth-resolving mode can be successfully applied only under dark conditions since daylight background contaminates the weak signal contributions detected from deeper water layers. The results presented in the following pages are derived from depth resolved data which have been numerically integrated. This is equivalent to the data of a depth-integrating laser fluorosensor.

#### 4.1. Instrument description

An Xenon Chloride (XeCl) excimer laser emitting at 308 nm serves as the main light source. Front and rear laser outputs are utilized as a lidar beam, or as a pumping beam for the dye laser tuned to an emission at 450 nm. The signal receiver is a Schmidt-Cassegrain telescope. Its optical axis is almost co-axial with the laser beams and the 5 mrad field of view corresponds to the excimer laser beam divergence. Dichroic beamsplitters deflect selected spectral ranges of the telescope output to optical filters and gated photomultipliers. Three selectable signals are sequentially combined on one signal line and fed to a one-channel fast transient recorder.

The laser and the detector system are mounted on an optical table to obtain a rigid alignment of the optical setup (figure 8). System operation is done in-flight by one operator. A microcomputer controls laser selection, triggering and power, selection of different detection wavelengths, quick look data output and auxiliary functions such as photcamera activation and recording of global radiation data.

#### 4.2. Hydrographic measurements

Monochromatic irradiation of natural seawater yields spectral structures (figure 9) which are related to (i) Rayleigh and Mie scattering of molecules and particles, (ii) Raman scattering of water with a wave number shift of  $3400 \text{ cm}^{-1}$ , (iii) fluorescence of Gelbstoffe (dissolved organic matter) and (iv) fluorescence of chlorophyll-a. Assuming an optical deep and homogeneous water column, and starting from the hydrographic lidar equation, the interpretation of time-integrated signals returns (Browell 1977) obtained from the inelastic spectral structures (ii)-(iv) yields a detected power:

$$P_R \sim H^{-2} \sigma_R / (k_{ex} + k_R)$$

for water Raman scattering and

$$P_F \sim H^{-2} \sigma_F / (k_{ex} + k_F)$$

for Gelbstoffe or chlorophyll-a fluorescence.  $H$  describes the flight height, parameters  $\sigma$  the quantum efficiencies of water Raman scatter and fluorescence and parameters  $k$  the attenuation coefficient at the excitation, Raman scatter or fluorescence wavelengths, each of which is denoted with the respective subscript.  $\sigma_R$

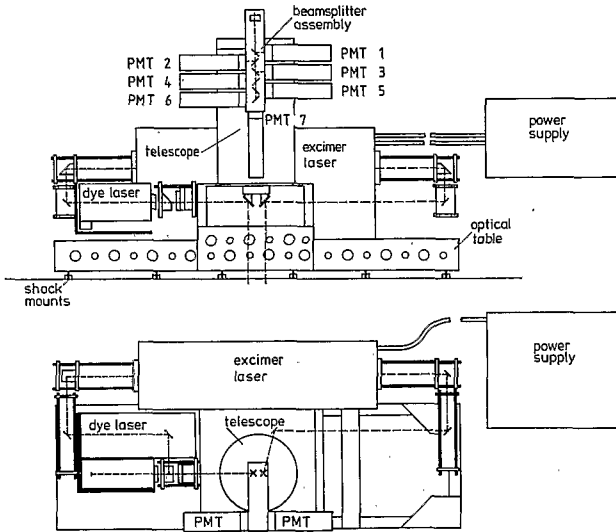


Figure 8. Optical part of the Oceanographic Lidar System. Position of the telescope is above a bottom hatch of the aircraft for free field of view to the water surface. Only three of seven photomultipliers are shown.

can be set to the constant approximately and the Raman signal intensity reflects the inverse sum of attenuation coefficients at the laser and the Raman wavelengths. Using the two lasers installed in OLS with 308 and 450 nm emission, water Raman signals are observed at 344 and 533 nm, and the following data are derived:

$$\text{UV attenuation coefficient} = k(308) + k(344) \sim 1/P_R(344)$$

$$\text{VIS attenuation coefficient} = k(450) + k(533) \sim 1/P_R(533).$$

Gelbstoffe or chlorophyll fluorescence signal power  $P_F$  reads:

$$P_F \sim \sigma_F / (k_{ex} + k_F)$$

which, after normalizing to the water Raman scatter signal, yields:

$$P_F/P_R = \sigma_F / \sigma_R (k_{ex} + K_R) / (k_{ex} + K_F).$$

In this equation  $\sigma_F$  is the only variable parameter if the ratio  $(K_{ex} + k_R) / (k_{ex} + k_F)$  can be set to be a constant (Bristow *et al.* 1981). This requires a spectrally close selection of excitation and detection wavelengths. Fluorescent matter concentrations derived with OLS then read:

$$\text{Gelbstoff} = F(366)/R(344)$$

$$\text{Chlorophyll} = F(685)/R(533)$$

obtained with 308 and 450 nm excitations, respectively. Although being given in dimensionless units, these parameters represent absolute quantities in terms of efficiencies of fluorescent compounds normalized to the constant water Raman efficiency.

As an example of the oceanographic campaigns performed with the OLS, some results obtained in the experiment 'Fronten II' in October 1985 in the German Bight are presented. The experiment aimed at an investigation of characteristic water masses and fronts in this area and was performed jointly by oceanographers from the Alfred Wegener Institute for Polar and Marine Research, Bremerhaven, and from institutes of the University of Hamburg and by the remote sensing group of the University of Oldenburg.

It could be shown in this experiment that the distribution of Gelbstoffe obtained with the OLS provides an efficient method to describe river plume fronts in the German Bight caused by the freshwater input of the rivers Elbe and Weser (Reuter *et al.* 1986).

Two fronts of this type were identified. Their positions and the location of the water masses separated by these fronts are shown in figure 10. This map has been derived from data of four flights over a period of three days and with the support of shipboard sea measurements. The lower limit of sensitivity of the airborne Gelbstoffe measurement is almost the same as with laboratory instrumentation.

Airborne Gelbstoffe data were compared with salinity measured in the surface layer at identical ship and aircraft positions, whereby the difference of the sampling time of data chosen for this purpose did not exceed one hour. The covariance of these parameters is high, which is typical of the German Bight, with a correlation coefficient of  $-0.96$ .

To describe further the hydrographic situation derived with the OLS, profiles of the UV and VIS attenuation coefficients, and Gelbstoffe and Chlorophyll obtained on 4 October 1984 on latitude  $54^{\circ}\text{N}$  and  $54^{\circ}15'\text{N}$ , are shown in figures 11 and 12.

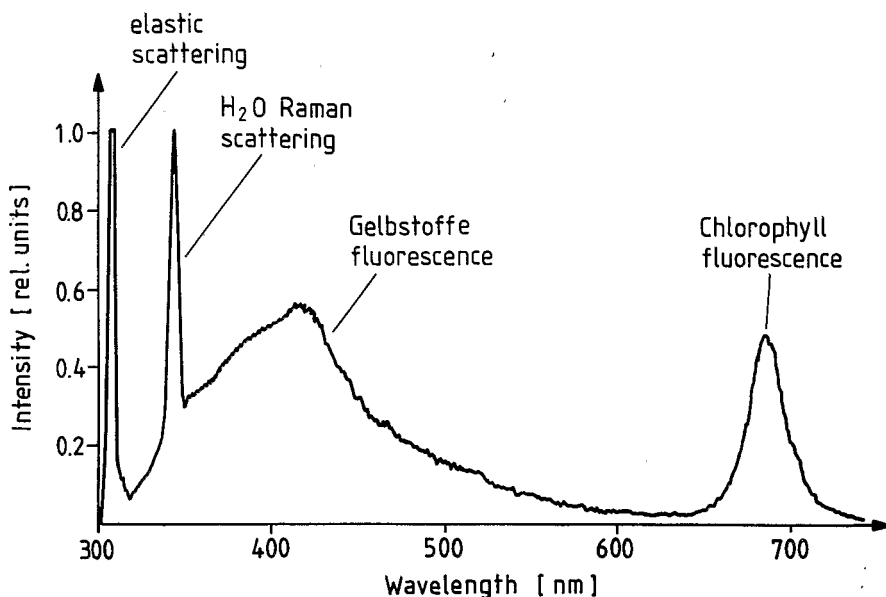


Figure 9. Emission spectrum of a water sample taken from the German Bight. Excitation wavelength is 308 nm. Gelbstoffe represents dissolved organic matter in seawater, being of natural origin and brought to the sea by river runoff. Chlorophyll-a fluorescence is used to determine phytoplankton.

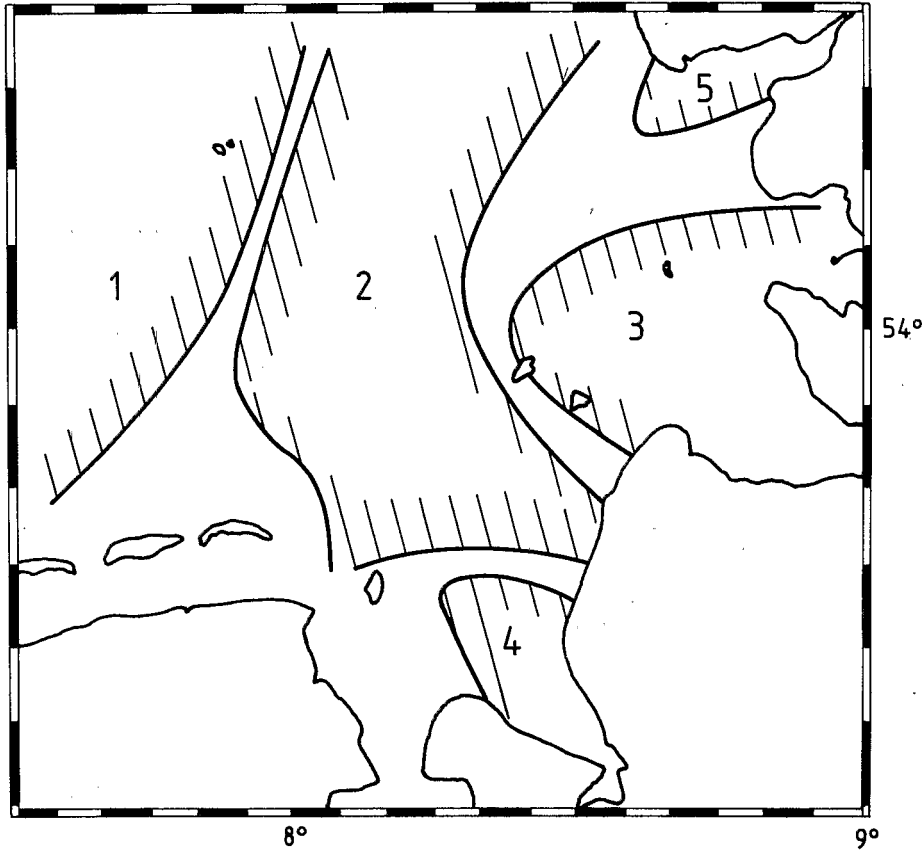


Figure 10. Characteristic water types in the German Bight derived from airborne Gelbstoffe fluorescence and shipboard salinity data on 3–5 October 1985. Type 1 represents open sea water, type 2 is produced by mixing of open sea and river water, types 3, 4 and 5 correspond to runoff of rivers Elbe, Weser and Eider.

The formation of water types 1, 2, 3 and 5 separated by frontal transition areas can be clearly seen in the Gelbstoffe data. According to the shipboard sea measurements, chlorophyll concentration is low, being in the order of a few microgram per litre, and this parameter did not obviously correlate with the other parameters measured.

#### 4.3. Investigation of oil spills

The potential of the hydrographic lidar for the identification and analysis of oil films on the sea surface has been studied by various research groups in detail, see, for example, O'Neil *et al.* (1980) and Burlamacchi *et al.* (1983). The dependance of the signal return on the fluorescence efficiency and the film thickness (Kung and Itzkan 1975, Visser 1979, Hoge 1983), as well as the attenuation of water raman scatter from the underlying water column (Hoge and Swift 1980), have been utilized for the purpose of quantifying spill volumes.

flight number : 083  
date : 04-OCT-86

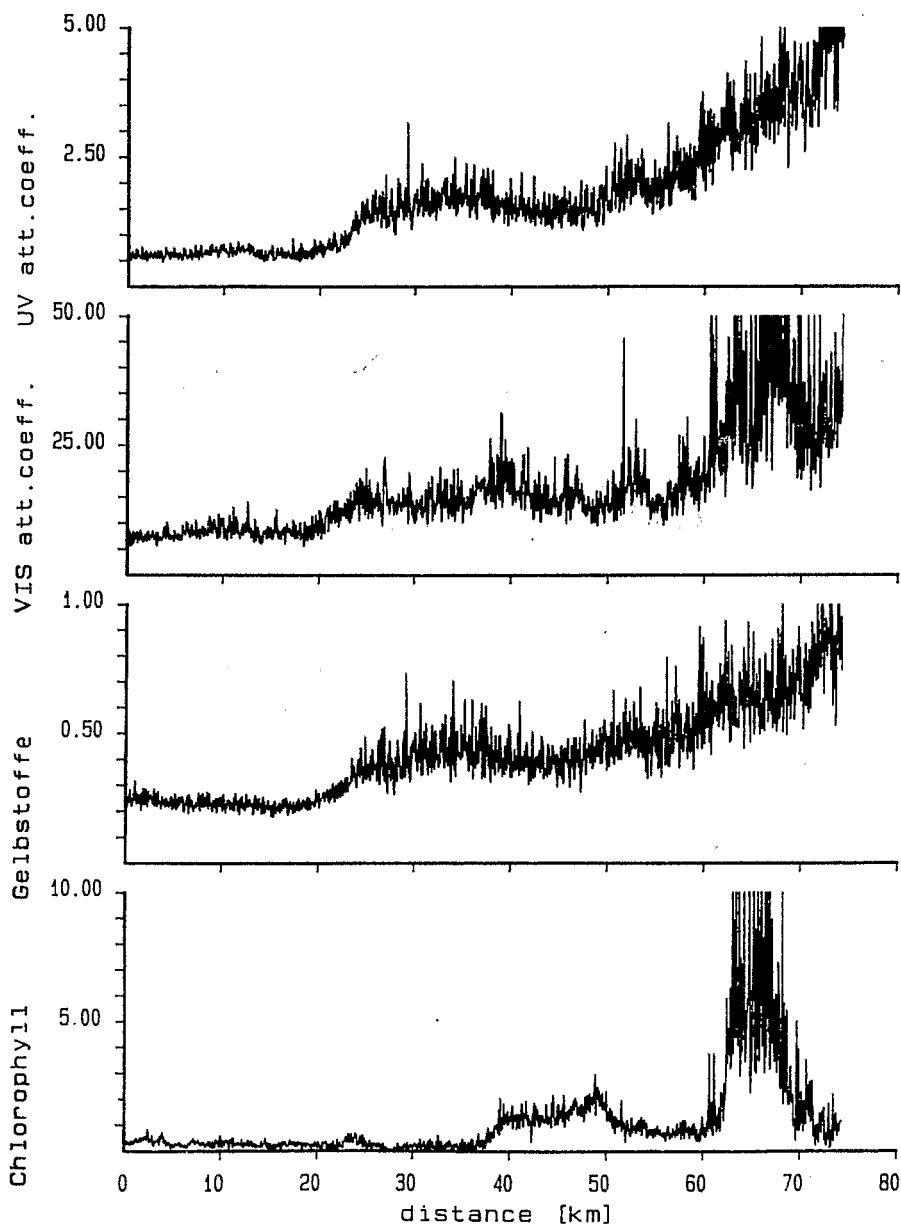


Figure 11. West-east section on  $54^{\circ}15'N$  from  $7^{\circ}40'E$  to  $8^{\circ}50'E$ , 4 October 1985. The front separating water types 1 and 2 is located around 22 km, being about 7 km wide. Water type 5, river Eider runoff, is marked by a drastic increase in Gelbstoffe and turbidity and a strong plankton bloom is identified in this area from the high Chlorophyll data.

flight number :081  
date :04-OCT-85

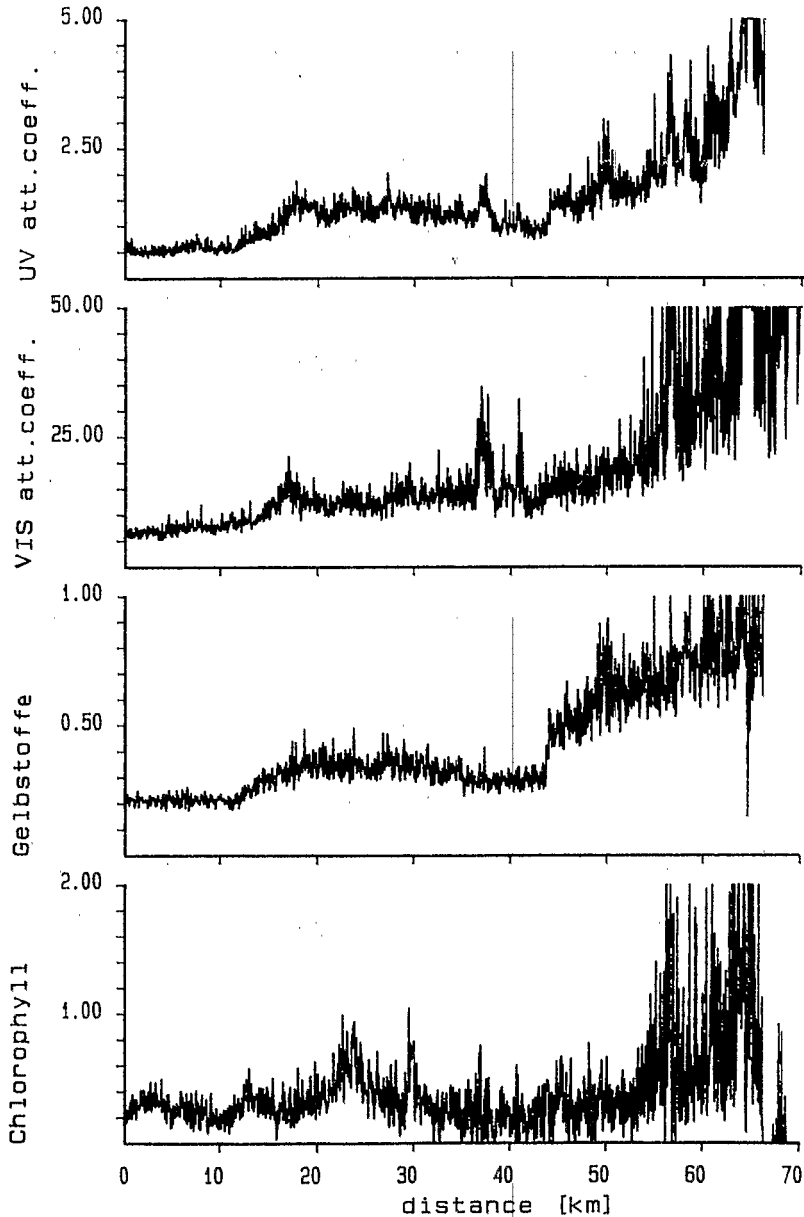


Figure 12. West-east section on  $54^{\circ}00'N$  from  $7^{\circ}40'E$  to  $8^{\circ}45'E$ , 4 October 1985. The fronts separating water types 1 and 2, and water types 2 and 3, are located around 13 km and 43 km, respectively.

It has been the goal of airborne campaigns performed with OLS to investigate the capabilities of deriving information typically on oil spills following controlled discharges by ship traffic or off-shore platforms. In these cases the amount of oil is mostly small as compared to accidental spills, giving rise to a film thickness in the order of a few micrometers only.

This situation was simulated in the Marine Pollution (MARPOL) exercise north-west of Rotterdam on 7 May 1986, in co-operation with Rijkswaterstat, The Netherlands (Diebel *et al.* 1989). A moving vessel discharged 60 litres of oil per nautical mile, mixed with  $100 \text{ m}^3$  of sea water prior to spilling. Two types of oil were utilized: a mixture of gasoil, fuel, lubrication and crude oil (here referred to as crude oil) and a diesel fuel.

The results of an OLS overflight, 30 min after crude oil discharge and 3 min after the start of diesel discharge, are shown in figure 13. Outside the oil spill water Raman scatter and Gelbstoff fluorescence are measured. Over the spills these signals are altered by absorption and fluorescence of the oil. The strong fluorescence of the crude oil at blue, green and red wavelengths is very obvious at the near-distance of 4000m in figure 13. In contrast to this, the diesel yields a strong signal at UV wavelengths at a distance of 5000m. The film thickness derived from the depression of water Raman scatter yields data that are considered to be realistic with the amount of oil spilled.

Data obtained in an overflight of the same spills about 30 min later (figure 14) show a depression of the signal intensity in all detection channels, more pronounced

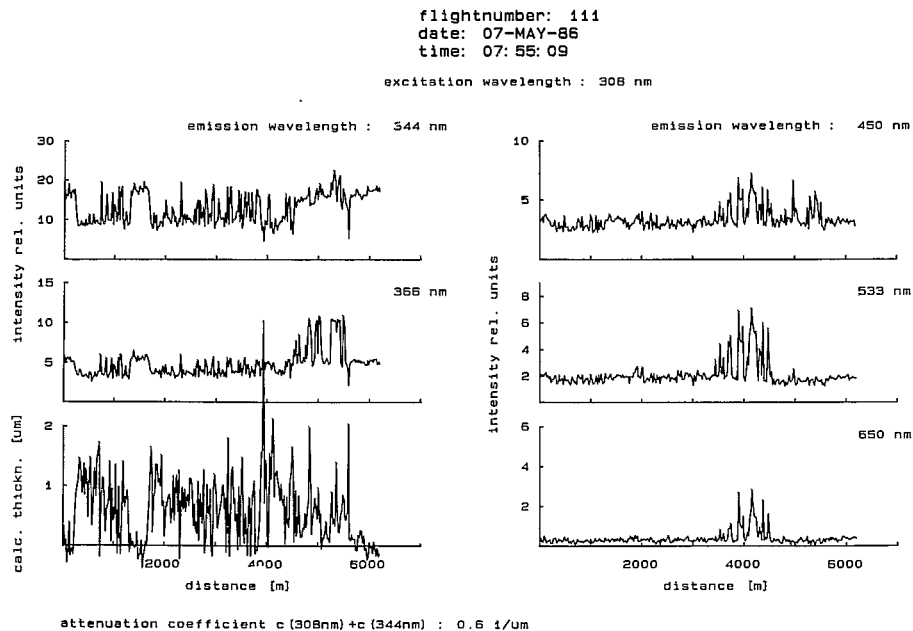


Figure 13. Profiles obtained at various emission wavelengths from a crude oil and a diesel spill, both discharged with a quantity of 60 l./n.m. Crude oil begins at position 500 m. Crude oil ends, and diesel fuel begins, at position 4600 m. Ship position is at 5700 m. The profile of film thickness calculated from these data is displayed on the left lowest trace.

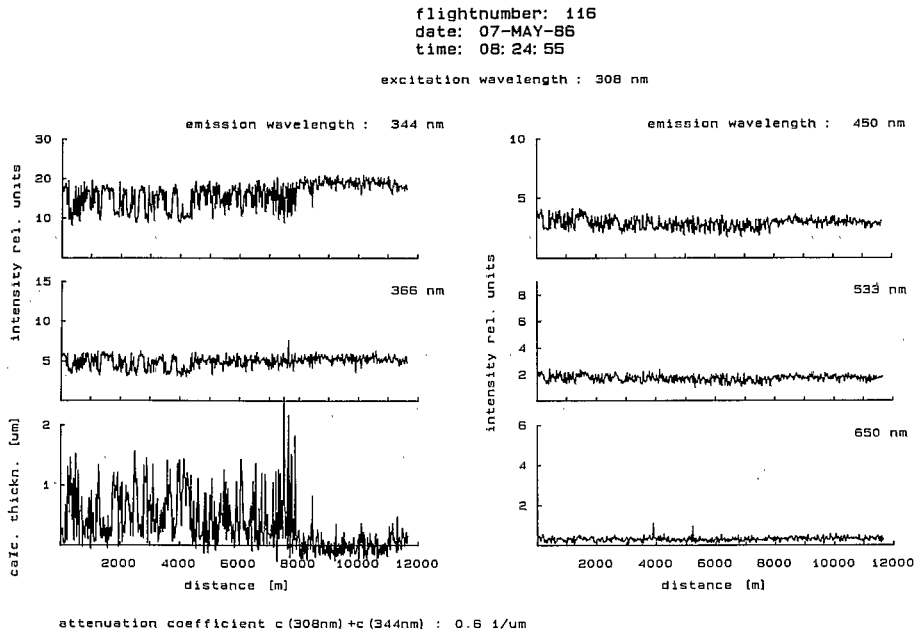


Figure 14. Same situation as shown in Figure 13, 30 min later. Crude oil begins at position 200 m. Crude oil ends, and diesel fuel begins, at position 4500 m. Diesel ends at position 8000 m.

in the UV than at higher wavelengths. The characteristic fluorescence signature of the oils is lost. This effect is most probably associated with evaporation of fluorescent oil compounds due to windspeeds of about 5 kt. However, the bulk of the oil films is still present. The calculated film thickness has only slightly decreased when compared to the data shown in figure 13. This finding is also supported by visual inspection. A marked alteration of the spills could not be made out within the period of overflights.

It is concluded that the fluorescent compounds of mineral oil are affected to a higher degree than other surface-active components. This limits fluorometric fingerprinting of small discharges of mineral oil if identification of the type of oil is of primary interest.

## 5. General conclusions

Aircraft experiments in the past fifteen years began using sensors working in the visible and infrared wavelengths. Later most of the research work was done in the microwave part of the spectrum but, fortunately, some teams all over Europe and the rest of the world have continued their investigations in the visible and infrared. A new generation of sensors appeared during recent years showing great promise for dedicated applications because of developments in microelectronics and optics and because active optical sensors have been improved in order to be more reliable, lighter and usable in airborne environments.

This development of new generation sensors is strongly supported by the highest remote sensing authorities and, as an example, a joint ESA/Earth Observation Planned Programme (EOPP), and Joint Research Centre (JRC) of the European Communities experiment called the European Imaging Spectroscopy Aircraft Cam-

paign (EISAC), has been conducted from 15 May to 15 June 1989 using passive multispectral push-broom imagers over five European countries. Scientists of six countries have participated working on thematic applications ranging from forestry to oceanography, from soils to agriculture and with promising first-look results.

No effort has been wasted, during these early years of remote sensing, in the visible and infrared spectrum and it is suggested that the new developments under way are to be closely monitored.

## References

- BRISTOW, M., NIELSEN, D., BUNDY, D., and FURTEK, R., 1981, Use of water Raman emission to correct airborne laser fluorosensor data for effects of water optical attenuation. *Applied Optics*, **20**, 2889-2905.
- BROWELL, E. V., 1977, Analysis of laser fluorosensor systems for remote algae detection and quantification. Technical Note, National Aeronautics and Space Administration (Hampton: NASA), TND-8447.
- BURLAMACCHI, P., CECCHI, G., MAZZINGHI, P., and PANTANI, L., 1983, Performance evaluation of UV sources for Lidar fluorosensing of oil films. *Applied Optics*, **22**, 48-53.
- COLWELL, R. N. (editor) 1983, *Manual of Remote Sensing* (Falls Church: American Society of Photogrammetry).
- DIEBEL, D., 1987, *Tiefenaufgelöste Laserfernerkundung geschichteter Strukturen im Meer unter Verwendung von Gelbstoff als Tracersubstanz*. PhD Thesis (Germany: University of Oldenburg).
- DIEBEL-LANGOHR, D., HENGSTERMANN, T., and REUTER, R., 1986, Water depth resolved determination of hydrographic parameters from airborne lidar measurements. *Marine Interface Hydrodynamics*, edited by J. C. J. Nichoul (Amsterdam: Elsevier), 591-602.
- DIEBEL, D., HENGSTERMANN, T., REUTER, R., and WILKOMM, R., 1989, Laser fluorosensing of mineral oil spills. *Institute of Petrol Conference on the Remote Sensing of Oil Slicks*, edited by A. E. Lodge (Chichester: Wiley), 127-142.
- HOGUE, F. E., 1983, Oil film, thickness using airborne laser-induced oil fluorescence backscatter. *Applied Optics*, **22**, 3316-3317.
- HOGUE, F. E., and SWIFT, R. N., 1980, Oil film thickness measurement using airborne laser-induced water Raman backscatter. *Applied Optics*, **19**, 3269-3281.
- KUNG, R. T. V., and ITZKAN, I., 1975, Absolute oil fluorescence conversion efficiency. *Applied Optics*, **15**, 409-415.
- LOOYEN, W. J., VAN SWOL, R. W., BIJLSMA, R. J., CLEVERS, J. G. P. W., VAN KASTEREN, H. W. J., MEULSTEE, C., PELLEMAND, A. H. J. M., and DONZE, M., 1989, CAESAR: performance and possibilities. Blied Commissie Remote Sensing (Delft: BCRS), 06.
- MARSAC, F., PETIT, M., and STRETTA, J. M., 1987, Radiométrie aérienne et prospection thonière a L'ORSTOM. Méthodologie, Bilan et Prospective. Institut Français de Recherche Scientifique Pour le Développement en Coopération Conference "Télé-détection 12" Collection Initiations-documents technique (ORSTOM, Paris), No. 68.
- MASSIN, J. M., 1978, Remote Sensing for the Control of Marine Pollution. Preliminary Inventory of available technologies. Committee on the Challenges of Modern Society Report to the North Atlantic Treaty Organisation (CCMS, Washington/Paris), No. 78.
- O'NEIL, R. A., BUJA-BIJUNAS, L., and RAINER, D. M., 1980, Field performance of a laser fluorosensor for the detection of oil spills. *Applied Optics*, **19**, 863-870.
- POUWELLS, H., 1987, Users guide to CAESAR. Blied Commissie Remote Sensing (BCRS, Delft), 04.
- REUTER, R., DIEBEL-LANGOHR, D., DOERRE, F., and HENGSTERMANN, T., 1986, Airborne laser fluorosensor measurement of Gelbstoff. Final report to the European Space Agency on The Influences of Gelbstoff on Remote Sensing of Seawater Constituents from Space (Forschungszentrum Geesthacht GmbH), Contract No. RFQ 3-5060/84/NL/MD.
- VAN VALKENBURG, A. L. G., 1985, Description of Calibration Procedure of CAESAR (Technisch Physische Dienst, Technical Research Centre, Delft).
- VISSER, H., 1979, Télédétection of the thickness of oil films on polluted water based on the oil fluorescence properties. *Applied Optics*, **18**, 1746-1749.